DNA Self-Assembly

DOI: 10.1002/anie.201203875

Controlling the Chirality of DNA Nanocages**

Chuan Zhang, Weimin Wu, Xiang Li, Cheng Tian, Hang Qian, Guansong Wang, Wen Jiang, and Chengde Mao**

We report a rational approach for controlling the chirality of self-assembled DNA nanocages at the nanoscale. Chirality on the nanoscale originates from the asymmetric characteristics of the component DNA building block (DNA nanomotif), but is distinct from the intrinsic, molecular-level chirality of the DNA duplex. By purposely removing two-dimensional (2D) rotation symmetry from the DNA nanomotif, we can control the three-dimensional (3D) chirality of the DNA nanocages. Such chiral control would be useful for tuning the photonic/optical properties of nanophotonic devices when DNA nanostructures are used as structural scaffolds.[1–3]

Chirality is an important structural feature across all size scales, from molecules to galaxies. Nanoscaled (1–100 nm) chirality bridges between the intrinsic chirality of molecules and the macroscale chirality of materials. Chemical synthesis and stereo-selective separation readily allow preparation of chiral molecules, and advanced fabrication methods can be used to fabricate chiral structures at the micrometer scale. However, there is a gap between these two approaches, how to rationally design and prepare chiral objects at the nanometer scale (1–100 nm). Such nanoscaled chiral structures have many technological applications, for example, chiral plasmonic devices.[4–6] Biomimetic, supramolecular DNA self-assembly is a powerful technique for building nanostructures because of its programmability and well-established secondary structure.[7–9]

[*] C. Zhang, X. Li, C. Tian, H. Qian, C. Mao
Department of Chemistry, Purdue University
West Lafayette, IN 47907 (USA)
E-mail: mao@purdue.edu
W. Wu, W. Jiang
Department of Biological Sciences, Purdue University (USA)
H. Qian
College of Chemistry and Chemical Engineering, Xiamen University (China)
G. Wang
The Institute of Respiratory Diseases, Xinqiao Hospital
Chongqing 400037 (China)
E-mail: wanggs2003@hotmail.com

[**] This work was supported by the Office of Naval Research and the National Science Foundation of China (No. 81028001). DLS and AFM studies were carried out in the Purdue Laboratory for Chemical Nanotechnology (PLCN). The cryo-EM images were taken in the Purdue Biological Electron Microscopy Facility and the Purdue Rosen Center for Advanced Computing (RCAC) provided the computational resource for the 3D reconstructions.

Supporting information for this article (experimental details) is available on the WWW under http://dx.doi.org/10.1002/anie.201203875.

DNA nanocages[10–22] are intrinsically chiral at the molecular level, because DNA duplexes are chiral. In addition, the geometric folding, twisting, bending, and association of the component DNA duplexes in DNA nanostructures could also lead to nanoscaled chiral features.[14] Turberfield and co-workers investigated the chiral property of a DNA tetrahedron.[13] Yan and co-workers used L-DNA, instead of D-DNA, to change the chirality of DNA nanotubes.[23] We have previously assembled a DNA octahedron with chiral features out of symmetric four-point-star motif.[24] A cryogenic electron microscopy (cryoEM) image with 12 Å resolution revealed a chiral structure (strut twisting) of the octahedron. Though being unambiguously observed, the degree of strut twisting was small. It remains a challenge to rationally control the extent and direction of the nanoscaled chirality in tile-based DNA nanocages. Herein, we report a simple strategy to overcome this problem and have demonstrated this through the construction of a series of DNA triangular prisms with different chiralities.

A triangular prism consists of six copies of identical asymmetric three-point-star motifs (Figure 1) which are related to one another by D_3 symmetry associated with the prism; a threefold rotational axis goes through the centers of the triangular faces, and three twofold rotational axes are perpendicular to the threefold rotational axes and go through the centers of vertical struts. The six horizontal struts of the top and bottom triangular faces are related by the D_3 symmetry and identical. The three vertical struts along the side faces are related by the threefold rotational symmetry, thus identical to each other. However, the horizontal struts and the vertical struts are not related to each other by symmetry, and are thus different. To satisfy the overall symmetry, the three-point-star motif has no symmetry, and all of its seven component strands have unique sequences. Two branches of the motif have complementary sticky ends. Their association (from two horizontally adjacent motifs) leads to formation of the horizontal struts of the triangular faces. The third branch has self-complementary sticky ends. Their association (from two vertically adjacent motifs) forms a vertical strut along the side face.

The asymmetric three-point-star motif, as shown in Figure 1a, contains seven strands: one long, central strand (**C**; blue/red), three medium strands (**M1**, **M2**, and **M3**; green) and three short strands (**S1**, **S2**, and **S3**; black). The three single-stranded loops (**L1**, **L2**, and **L3**; red) of strand **C** at the center of the motif have different lengths to create the desired flexibility. In a triangular prism, the angle between two arms in the triangular faces is 60°, much smaller than that in the vertical, parallelogram face (approximately 90°). Thus the branches in the triangular faces have to bend more than the

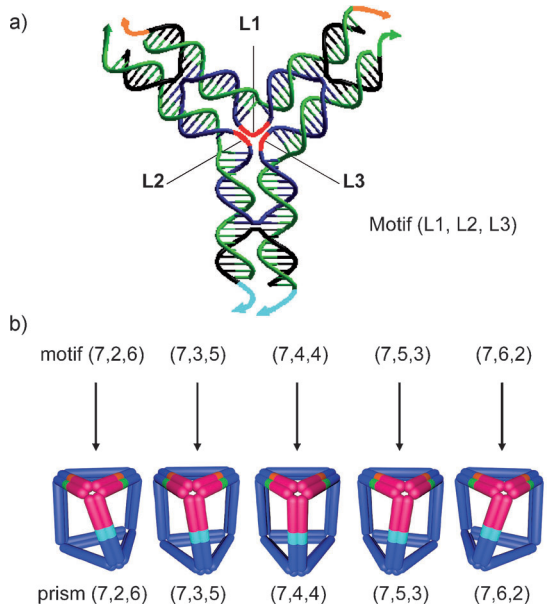

Figure 1. Self-assembly of chiral DNA triangular prisms out of asymmetric three-point-star motifs. a) Schematic representation of the asymmetric three-point-star motifs. **C** = blue/red; **M1**, **M2**, and **M3** = green; **S1**, **S2**, and **S3** = black; **L1**, **L2**, and **L3** = red. For each motif, the two top branches have complementary sticky ends (green and yellow) and the bottom branch has self-complementary sticky ends (cyan). b) Scheme of the resulting chiral triangular prisms. In each prism, one component motif is highlighted. Note that the motifs and their resulting prisms are designated by the loop lengths in nucleotides.

branches in the parallelogram faces do. Because longer single-stranded loops provide more flexibility and allow the two embracing branches to bend more, the underlying geometric requirements dictate the lengths of the central loops: **L1** (seven nucleotides (nt)) has to be longer than **L2** and **L3** (2–6 nt). **L2** and **L3** face toward the parallelogram faces and can control the overall twist of the assembled prisms when their lengths are varied. When **L2** and **L3** have the same length (4 nt), both left and right sides of the motif bend equally, leading to formation of an untwisted, achiral prism (7,4,4). When **L2** and **L3** have different lengths, the two sides of the motif will bend to different extents, leading to twisted, chiral prisms. The larger the length difference between **L2** and **L3**, the stronger the chirality of the prism will be.

Prism assembly was performed according to previously reported methods.[24] Briefly, all component DNA strands were mixed at an equal molar ratio in a Mg^{2+}-containing, aqueous buffer with a neutral pH value. The mixture was heated and then slowly cooled from 95 °C to 25 °C over 48 hours. The assembled products were first examined by native polyacrylamide gel electrophoresis (PAGE). Bands corresponding to a molecular weight that was expected for triangular and tetragonal prisms were observed (see Supporting Information, Figure S1). When the DNA concentration was decreased to 100 nM or below, the triangular prism became the dominant assembly product (greater than 75 %). Although all the triangular prisms, twisted or untwisted, have the same molecular weight and strut length, they have different volumes because of the twisting. The untwisted, achiral prism (7,4,4) has the largest volume and was expected to have the slowest electrophoretic mobility. Twisted, chiral prisms (7,3,5) and (7,5,3) have smaller volumes and therefore, would have faster mobilities. The most twisted, chiral prisms (7,2,6) and (7,6,2) have the smallest volume and therefore, would have the fastest electrophoretic mobilities. The mobility difference was small, but was consistently and unambiguously observed in the native PAGE (Figure 2a) over multiple experiments. This mobility pattern was strongly correlated with the chiral characteristics of the DNA prisms.

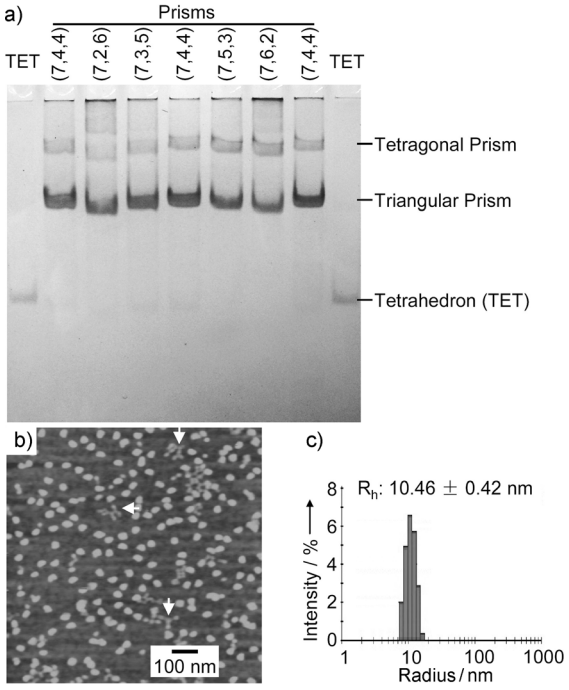

Figure 2. Characterization of the self-assembled DNA prisms by a) native polyacrylamide gel electrophoresis (PAGE), b) atomic force microscopy (AFM) on prism (7,4,4), and c) dynamic light scattering (DLS) on prism (7,4,4).

We further characterized all DNA triangular prisms by atomic force microscopy (AFM) and dynamic light scattering (DLS). AFM imaging confirmed that all DNA prisms were uniform in size (Figure 2b and Figure S2). Y-shaped motifs (arrows) were occasionally observed in the AFM images where the prisms disassembled during washing of the imaging sample, this result demonstrated that the nanoparticles were assembled out of three-point-star motifs. DLS was used to measure the hydrodynamic radii (R_h) of the assembled DNA prisms in solution. The R_h of the achiral prism (7,4,4) was approximately 10.46 ± 0.42 nm (Figure 2c), consistent with the theoretical radius (10.6 nm) calculated from the structural model assuming a pitch of 3.3 nm per turn and a diameter of 2 nm for DNA duplexes. The measured R_h of all the twisted, chiral triangular prisms (Table S1) were roughly the same as the R_h of the achiral prism, because the twisting only creates a small decrease in volume and DLS measurement is not sensitive enough to detect such subtle changes.

To clearly demonstrate the chiral characteristics of the assembled DNA triangular prisms, we used cryogenic electron microscopy (cryoEM) imaging in conjunction with a single-particle 3D reconstruction technique (Figure 3 and Figure S3–S7). In raw cryoEM micrographs, individual DNA particles showing the expected sizes were clearly visible. Projections of triangular shapes and tetragonal shapes could be easily found, which were consistent with the formation of triangular prisms. The prism edges appeared to be approximately 15 nm, as expected. From the randomly oriented, individual DNA particles observed in the cryoEM images, we reconstructed the native structures of the DNA complexes by single-particle 3D reconstruction, a well-developed technique in structural biology.[25] Triangular prism structures were revealed at resolutions of 24–30 Å. The 2D projections of the structural models matched very well with the raw cryoEM images, confirming that the reconstructed models were correct.

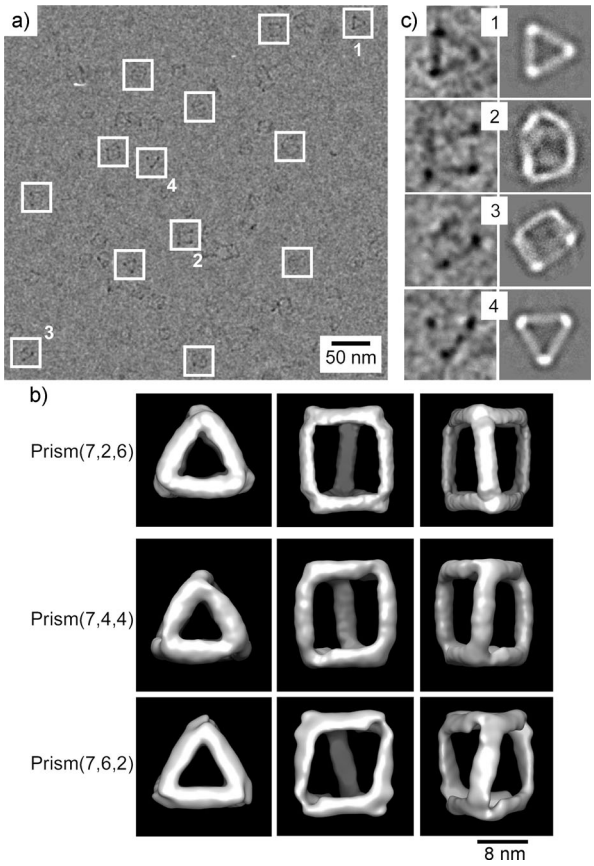

Figure 3. CryoEM characterization of the self-assembled DNA prisms. a) A raw cryoEM image of prism (7,4,4) and individual raw particles selected from the image (white boxes). b) The reconstructed 3D maps of DNA prisms. c) Comparison of cryoEM images of selected particles (left) and 2D projections from the reconstructed structural model (right) for prism (7,4,4).

The chiralities of the DNA prisms are clearly shown in the reconstructed structural models (Figure 3b). First, both prisms (7,6,2) and (7,2,6) are strongly twisted, but in opposite directions. This result confirms our hypothesis that varying the lengths of the central loops can control the chirality of the resulting DNA prism. Second, the prism (7,4,4) also exhibits slight chirality. This is not surprising as a similar feature has been observed in a previous report.[24] Such subtle chirality is attributed to the intrinsic structure of the three-point-motif and cannot be easily altered.

In conclusion, chiral DNA triangular prisms were successfully constructed using asymmetric DNA three-point-star motifs. During assembly, the free loops in the central strand not only provide flexibility for the bending of the branches but also control the chirality (extent and direction) of the final structure. These asymmetric motifs allow fabrication of more complex nanocages than did previous symmetric motifs.[26–30] We expect that the resulting chiral structures will provide useful architectures for nanodevices such as chiral metamaterials.[1–6]

Received: May 19, 2012
Published online: July 3, 2012

Keywords: chirality · DNA · nanocages · nanostructures · self-assembly

[1] A. Kuzyk, R. Schreiber, Z. Fan, G. Pardatscher, E. Roller, A. Högele, F. C. Simmel, A. O. Govorov, T. Liedl, *Nature* **2012**, *483*, 311 – 314.
[2] A. J. Mastroianni, S. A. Claridge, A. P. Alivisatos, *J. Am. Chem. Soc.* **2009**, *131*, 8455 – 8459.
[3] X. Shen, C. Song, J. Wang, D. Shi, Z. Wang, N. Liu, B. Ding, *J. Am. Chem. Soc.* **2012**, *134*, 146 – 149.
[4] K. J. Gansel, M. Thiel, M. S. Rill, M. Decker, K. Bade, V. Saile, G. von Freymann, S. Linden, M. Wegener, *Science* **2009**, *325*, 1513 – 1515.
[5] M. Hentschel, M. Schäferling, T. Weiss, N. Liu, H. Giessen, *Nano Lett.* **2012**, *12*, 2542 – 2547.
[6] Z. Li, Z. Zhu, W. Liu, Y. Zhou, B. Han, Y. Gao, Z. Tang, *J. Am. Chem. Soc.* **2012**, *134*, 3322 – 3325.
[7] N. C. Seeman, *Nature* **2003**, *421*, 427 – 431.
[8] N. C. Seeman, *Annu. Rev. Biochem.* **2010**, *79*, 65 – 87.
[9] C. Lin, Y. Liu, H. Yan, *Biochemistry* **2009**, *48*, 1663 – 1674.
[10] J. H. Chen, N. C. Seeman, *Nature* **1991**, *350*, 631 – 633.
[11] Y. W. Zhang, N. C. Seeman, *J. Am. Chem. Soc.* **1994**, *116*, 1661 – 1669.
[12] W. M. Shih, J. D. Quispe, G. F. Joyce, *Nature* **2004**, *427*, 618 – 621.
[13] R. P. Goodman, A. T. Schaap, C. F. Tardin, C. M. Erben, R. M. Berry, C. F. Schmidt, A. J. Turberfield, *Science* **2005**, *310*, 1661 – 1665.
[14] S. M. Douglas, H. Dietz, T. Liedl, B. Högberg, F. Graf, W. M. Shih, *Nature* **2009**, *459*, 414 – 418.
[15] A. Kuzuya, M. Komiyama, *Chem. Commun.* **2009**, 4182 – 4184.
[16] E. S. Andersen, M. Dong, M. M. Nielsen, K. Jahn, R. Subramani, W. Mamdouh, M. M. Golas, B. Sander, H. Stark, C. L. P. Oliveira, J. S. Pedersen, V. Birkedal, F. Besenbacher, K. V. Gothelf, J. Kjems, *Nature* **2009**, *459*, 73 – 76.
[17] Y. G. Ke, J. Sharma, M. H. Liu, K. Jahn, Y. Liu, H. Yan, *Nano Lett.* **2009**, *9*, 2445 – 2447.
[18] Z. Li, B. Wei, J. Nangreave, C. Lin, Y. Liu, Y. Mi, H. Yan, *J. Am. Chem. Soc.* **2009**, *131*, 13093 – 13098.
[19] F. A. Aldaye, H. F. Sleiman, *J. Am. Chem. Soc.* **2007**, *129*, 13376 – 13377.
[20] D. Bhatia, S. Mehtab, R. Krishnan, S. S. Indi, A. Basu, Y. Krishnan, *Angew. Chem.* **2009**, *121*, 4198 – 4201; *Angew. Chem. Int. Ed.* **2009**, *48*, 4134 – 4137.

[21] F. F. Andersen, B. Knudsen, C. L. P. Oliveira, R. F. Frøhlich, D. Krüger, J. Bungert, M. Agbandje-McKenna, R. McKenna, S. Juul, J. Koch, J. L. Rubinstein, B. Guldbrandtsen, M. S. Hede, G. Karlsson, A. H. Andersen, J. S. Pedersen, B. R. Knudsen, *Nucleic Acids Res.* **2008**, *36*, 1113 – 1119.
[22] J. Zimmermann, M. P. J. Cebulla, S, Mönninghoff, G. von Kiedrowski, *Angew. Chem.* **2008**, *120*, 3682 – 3686; *Angew. Chem. Int. Ed.* **2008**, *47*, 3626 – 3630.
[23] C. Lin, Y. Ke, Z. Li, J. H. Wang, Y. Liu, H. Yan, *Nano Lett.* **2009**, *9*, 433 – 436.
[24] Y. He, M. Su, P. Fang, C. Zhang, A. E. Ribbe, W. Jiang, C. Mao, *Angew. Chem.* **2010**, *122*, 760 – 763; *Angew. Chem. Int. Ed.* **2010**, *49*, 748 – 751.
[25] S. J. Ludtke, P. R. Baldwin, W. Chiu, *J. Struct. Biol.* **1999**, *128*, 82 – 97.
[26] Y. He, Y. Tian, Y. Chen, Z. Deng, A. E. Ribbe, C. Mao, *Angew. Chem.* **2005**, *117*, 6852 – 6854; *Angew. Chem. Int. Ed.* **2005**, *44*, 6694 – 6696.
[27] Y. He, Y. Chen, H. Liu, A. E. Ribbe, C. Mao, *J. Am. Chem. Soc.* **2005**, *127*, 12202 – 12203.
[28] Y. He, T. Ye, M. Su, C. Zhang, A. E. Ribbe, W. Jiang, C. Mao, *Nature* **2008**, *452*, 198 – 201.
[29] C. Zhang, M. Su, Y. He, X. Zhao, P. Fang, A. E. Ribbe, W. Jiang, C. Mao, *Proc. Natl. Acad. Sci. USA* **2008**, *105*, 10665 – 10669.
[30] C. Zhang, S. H. Ko, Y. Leng, A. E. Ribbe, W. Jiang, C. Mao, *J. Am. Chem. Soc.* **2009**, *131*, 1413 – 1415.

